University of Groningen

Hepatic stellate cells induce an inflammatory phenotype in Kupffer cells via the release of extracellular vesicles

Geng, Yana; Wang, Junyu; Serna-Salas, Sandra Alejandra; Villanueva, Alejandra Hernández; Buist-Homan, Manon; Arrese, Marco; Olinga, Peter; Blokzijl, Hans; Moshage, Han

IMPORTANT NOTE: You are advised to consult the publisher's version (publisher's PDF) if you wish to cite from it. Please check the document version below.

Document Version
Publisher's PDF, also known as Version of record

Publication date:
2023

Link to publication in University of Groningen/UMCG research database

RESEARCH ARTICLE

Journal of Cellular Physiology WILEY

Hepatic stellate cells induce an inflammatory phenotype in Kupffer cells via the release of extracellular vesicles

Yana Geng[1,2] | Junyu Wang[1] | Sandra Alejandra Serna-Salas[1] |
Alejandra Hernández Villanueva[1,3] | Manon Buist-Homan[1,4] | Marco Arrese[3] |
Peter Olinga[2] | Hans Blokzijl[1] | Han Moshage[1,4]

[1]Department of Gastroenterology and Hepatology, University Medical Center Groningen, University of Groningen, Groningen, The Netherlands

[2]Department of Pharmaceutical Technology and Biopharmacy, Groningen Research Institute of Pharmacy, University of Groningen, Groningen, The Netherlands

[3]Department of Gastroenterology, Pontificia Universidad Católica de Chile, Santiago de Chile, Chile

[4]Department of Laboratory Medicine, University Medical Center Groningen, University of Groningen, Groningen, The Netherlands

Correspondence
Yana Geng and Han Moshage, Department of Gastroenterology and Hepatology, University Medical Center Groningen, Hanzeplein 1, 9713 GZ Groningen, The Netherlands.
Email: yana.geng@rug.nl and a.j.moshage@umcg.nl

Funding information
China Scholarship Council,
Grant/Award Numbers: 201506210062, 202006250036

Abstract

Liver fibrosis is the response of the liver to chronic liver inflammation. The communication between the resident liver macrophages (Kupffer cells [KCs]) and hepatic stellate cells (HSCs) has been mainly viewed as one-directional: from KCs to HSCs with KCs promoting fibrogenesis. However, recent studies indicated that HSCs may function as a hub of intercellular communications. Therefore, the aim of the present study was to investigate the role of HSCs on the inflammatory phenotype of KCs. Primary rat HSCs and KCs were isolated from male Wistar rats. HSCs-derived conditioned medium (CM) was harvested from different time intervals (Day 0−2: CM-D2 and Day 5−7: CM-D7) during the activation of HSCs. Extracellular vesicles (EVs) were isolated from CM by ultracentrifugation and evaluated by nanoparticle tracking analysis and western blot analysis. M1 and M2 markers of inflammation were measured by quantitative PCR and macrophage function by assessing phagocytic capacity. CM-D2 significantly induced the inflammatory phenotype in KCs, but not CM-D7. Neither CM-D2 nor CM-D7 affected the phagocytosis of KCs. Importantly, the proinflammatory effect of HSCs-derived CM is mediated via EVs released from HSCs since EVs isolated from CM mimicked the effect of CM, whereas EV-depleted CM lost its ability to induce a proinflammatory phenotype in KCs. In addition, when the activation of HSCs was inhibited, HSCs produced less EVs. Furthermore, the proinflammatory effects of CM and EVs are related to activating Toll-like receptor 4 (TLR4) in KCs. In conclusion, HSCs at an early stage of activation induce a proinflammatory phenotype in KCs via the release of EVs. This effect is absent in CM derived from HSCs at a later stage of activation and is dependent on the activation of TLR4 signaling pathway.

KEYWORDS
extracellular vesicles, hepatic stellate cells, inflammation, Kupffer cells, toll-like receptor 4

1 | INTRODUCTION

Hepatic stellate cells (HSCs) are key effector cells in the pathogenesis of liver fibrosis. In normal conditions, HSCs display the quiescent phenotype, manifested by the abundant presence of lipid droplets containing vitamin A, low production of extracellular matrix (ECM) components, and low proliferation rate. Following chronic liver injury, HSCs become activated and transdifferentiate into myofibroblast-like cells, losing lipid droplets, enhancing proliferation and migration, producing excessive amounts of ECM proteins and releasing proinflammatory and pro-fibrotic factors (Lee et al., 2015; Xu et al., 2012). The activation of HSCs is a multifactorial process, which is closely related to the immune and inflammatory response to tissue damage. It is believed that the liver-resident macrophages-Kupffer cells (KCs)- and blood monocyte-derived macrophages contribute critically to the progression of liver fibrosis. Macrophages are highly plastic cells. Their polarization is customarily assigned to M1- or M2-phenotype. M1 macrophages demonstrate proinflammatory features, releasing cytokines and chemokines thus attracting monocytes from the circulation, whereas M2 macrophages display high phagocytic and/or pro-fibrotic traits demonstrated by increased expression of MRC1 and/or TGF-β1. Upon liver damage, KCs acquire the proinflammatory M1-phenotype that recruit monocytes and neutrophils to the liver thus favoring the activation of HSCs (Pellicoro et al., 2014; Xu et al., 2012). On the other hand, it has been shown that HSCs also have immunoregulatory properties, such as presenting antigens and showing phagocytic ability (Jiang et al., 2008; Viñas et al., 2003; Wang et al., 2023; Zhan et al., 2006). However, how HSCs interact with their microenvironment during activation, in particular with KCs and macrophages, is still not well elucidated, especially not with regard to the immunoregulatory aspect.

Extracellular vesicles (EVs) are a group of cell-derived membranous particles, which have been shown to be important in intercellular communication. Compelling evidence showed that EVs play important roles in both physiological and pathological processes. In the liver, EVs are released from both parenchymal and nonparenchymal cells and are implicated in liver diseases (Balaphas et al., 2019; Devaraj et al., 2022). EVs derived from fat-laden hepatocytes can enhance the activation of HSCs via shuttling miR-128-3p from hepatocytes to HSCs, thus suppressing PPAR-γ expression (Hernández, Geng, et al., 2020; Hernández, Reyes, et al., 2020; Inzaugarat et al., 2016; Povero et al., 2015). Endothelial cell-derived EVs induce HSC migration via activating the sphingosine 1-phosphate (S1P) signaling pathway in HSCs (Wang et al., 2015). Moreover, HSCs have also been shown to release EVs. HSC-derived EVs contain connective tissue growth factor (CCN2) (Charrier et al., 2014) and sequester platelet-derived growth factor receptor-α (PDGFRα) (Kostallari et al., 2018) thus promoting the progression of liver fibrosis. Virtually nothing is known about the effect of HSC-derived EVs on KCs and the inflammatory process in fibrogenesis. Therefore, in the present study, we aim to examine the communication from HSCs to KCs and understand the role of HSCs-derived EVs in the interaction between HSCs and KCs.

2 | MATERIALS AND METHODS

2.1 | Animals

Specified pathogen-free male Wistar rats were purchased from Charles River Laboratories Inc. Rats were housed under standard laboratory conditions with free access to standard laboratory chow and water. All experiments were performed according to the Dutch law on the welfare of laboratory animals and guidelines of the ethics committee of the University of Groningen for care and use of laboratory animals.

2.2 | Cell isolation and culture

KCs and primary hepatocytes were isolated by two-step collagenase perfusion method as described previously (Geng et al., 2023; Moshage et al., 1990). KCs were collected from the supernatant of the post-hepatocyte fraction. The supernatant was centrifuged at 500g for 7 min and the pellet was resuspended in Hanks' Balanced Salt Solution (HBSS; Invitrogen) containing 0.3% BSA (HBSS/BSA). Then the suspension was centrifuged again at 500g for 7 min. The cell pellet was collected and resuspended in 8.5 mL HBSS/BSA and mixed with 3.2 mL Optiprep (Stemcell Technologies). After carefully mixing, the cell suspension was centrifuged at 1350g for 15 min. Then the layer of KCs was collected, resuspended in HBSS + 10% fetal calf serum (FCS) solution and seeded in cell culture plates. After the attachment period (around 10–15 min), nonadherent cells were removed and KCs were cultured in RPMI-1640 medium supplemented with 10% heat-inactivated FCS (HyClone) and 100 U/mL penicillin, 10 μg/mL streptomycin, and 250 ng/mL Fungizone (Lonza). Bright-field pictures were taken with digital light microscopy (Evos digital inverted microscope). CD68 and CD163 positive cells were recognized as KCs.

Primary HSCs were isolated by pronase (Merck) and collagenase-P (Roche) perfusion of the liver, followed by gradient centrifugation as described before (Moshage et al., 1990). HSCs were cultured in Iscove's Modified Dulbecco's Medium with Glutamax (Invitrogen) supplemented with 20% heat-inactivated FCS, 1 mmol/L sodium pyruvate (Invitrogen), 1× MEM non-essential amino acids (Invitrogen), 50 μg/mL gentamicin (Invitrogen), 100 U/mL penicillin, 10 μg/mL streptomycin, and 250 ng/mL Fungizone.

Hepatocytes were cultured in William's E medium (Invitrogen) supplemented with 50 μg/mL gentamicin. All cells were cultured at 37°C in a 5% (v/v) CO_2 condition.

HEK-Blue™ hTLR4 reporter cells (InvivoGen) were cultured in Dulbecco's modified Eagle's medium (Invitrogen) supplemented with 1% penicillin−streptomycin, 10% FCS, and 100 μg/mL normocin (Invitrogen). Fifty thousands cells per well were seeded in a 96-well cell culture plate in 100 μL of CM, 1:1 (v/v) mixed with HEK-Blue™ cell culture media, or in 100 μL of HEK-Blue™ cell culture media with 20 μg of EVs with or without the Toll-like receptor 4 (TLR4) inhibitor TAK242 (5 μmol/L) and then incubated for 24 h. For the detection of secreted alkaline phosphatase (SEAP) in response to TLR4 activation, 180 μL cell suspension was mixed with 20 μL HEK-Blue™ detection medium

(InvivoGen) in a new 96-well plate. The plate was incubated at 37°C for 2 h. Optical densities (OD) at 630 nm were read with a microplate reader (Bio-Tek Instruments, Inc.). The results were corrected by subtracting the values of wells without cells. Lipopolysaccharide (100 ng/mL) were included as a positive control.

2.3 | Preparation of conditioned medium (CM) and EVs

100,000 freshly isolated HSCs were seeded in T-175 polystyrene culture flasks (Corning). HSCs derived CM was harvested and subjected to differential ultracentrifugation as indicated in Figure 3a and as described before (Hernandez, Geng, et al., 2020). Briefly, CM-D2 and CM-D7 were obtained from Days 0 (excluding 4 h of attachment period) to 2 and from Days 5 to 7, respectively after initiation of HSC culture. Therefore, CM-D2 represents the CM derived from HSCs during their early activation phase, whereas CM-D7 represents the CM derived from HSCs during their relatively fully activated phase. EV-depleted CM-D2 (Depl-CM-D2) was obtained from CM-D2 after ultracentrifugation to remove EVs. CM-Hep was obtained from primary rat hepatocytes that were incubated for 24 h after isolation. All conditioned media were filtered through 0.2 μm sterile filter (Whatman) and stored at −80°C. Before treatment, CM was mixed with fresh KC medium at a 1:1 (v/v) ratio and then applied in experiments. KC medium mixed with HSC medium or hepatocyte medium at a 1:1 (v/v) ratio served as control media.

After differential ultracentrifugation, the EV fraction was resuspended in PBS and stored at −80°C. The amount of EVs was determined by the BCA protein assay method and EVs were subsequently diluted in KC medium to get a final concentration of 50 μg/ml.

2.4 | Immunofluorescence microscopy

For immunofluorescence staining, cells were seeded on coverslips. After treatment, cells were fixed, permeabilized and stained as described before (Geng, Hernández Villanueva, et al., 2020). Cells were incubated with anti-CD68 (Bio-Rad AbD Serotec) or anti-CD163 (Hycult Biotech) antibodies and labeled with secondary antibodies Alexa Fluor 488 (Invitrogen). Afterward, the coverslips were mounted in anti-fading mounting medium supplemented with DAPI (Vector Laboratories, Inc.). Images were captured using a Leica DMI6000 microscope and analyzed by ImageJ.

2.5 | RNA isolation and quantitative polymerase chain reaction

RNA was isolated and converted into cDNA as described before (Geng, Hernández Villanueva, et al., 2020). Quantitative real-time PCR was performed using the 7900HT Fast Real-time System (Applied Biosystems) using the TaqMan protocol. mRNA levels were normalized to 18S and then further normalized relative to

control groups. Sequences of primers and probes are shown in Supporting Information: Table 1.

2.6 | Phagocytosis assays

Phagocytic ability of KCs was assessed by quantification of uptake of fluorescein isothiocyanate (FITC)-labeled E. coli. FITC-labeled E. coli was produced by incubating formaldehyde-fixed E. coli with FITC (1 mg/mL; Sigma-Aldrich) for 1 h at room temperature. Bacterial concentration was determined by optical density at 600 nm (OD$_{600}$), assuming that an OD$_{600}$ of 1 equals 1×10^9 bacteria/mL. KCs were seeded on coverslips. After treatment, KCs were washed with PBS twice and then incubated with FITC-labeled E. coli at a 10:1 bacteria:cell ratio suspended in PBS, for 20 min at 37°C to allow internalization. Afterwards, cells were washed with PBS again to remove the non-internalized bacteria and then incubated with phalloidin (1:2000; Thermo Fisher Scientific) to stain F-actin for 30 min at room temperature. Afterwards, cells were washed again and the coverslips were mounted in anti-fading mounting medium supplemented with DAPI (Vector Laboratories, Inc.). Images were captured using a Leica DMI6000 microscope and analyzed with ImageJ. The numbers of bacteria were counted. The ones that were not internalized were excluded. Phagocytic ability was presented as the number of E. coli uptake per cell. The experiments were performed three times and data are presented as the mean ± SD.

2.7 | Western blot analysis and antibodies

The protein concentrations of samples were measured using the BCA protein Assay Kit (Thermo Fisher Scientific). EVs and cell lysates were loaded for SDS-PAGE and Western blot method was performed as described previously (Vrenken et al., 2008). Monoclonal antibodies against CD63 (Santa Cruz), Rab7 (Cell Signaling Technology), cytochrome-c (Cell Signaling Technology), α-tubulin (Sigma-Aldrich), collagen type 1 (Southern Biotech), α-SMA (Sigma-Aldrich), LC3B (Cell Signaling Technology), p62 (Cell Signaling Technology) were used to detect specific protein expression. The amount of proteins loaded was visualized with Ponceau S staining (Sigma-Aldrich). The immunoblots were quantified by densitometry from at least three independent experiments using ImageJ software.

2.8 | Nanoparticle tracking analysis (NTA)

The concentration and size distribution of particles were analyzed using a Nanosight NS300 unit (Malvern). All samples were diluted to provide a concentration of 1×10^8–1×10^9 particles/mL counts. All counts were performed in replicates of five for each sample, collecting 60 s videos with 300 valid tracks recorded per video (minimum of 1000 valid tracks recorded per sample). Nanosight 3.0 software was used for all analyses, using standard settings. The camera level for each sample was manually adjusted to achieve

optimal visualization of particles. To minimize variability, the camera level was set at 8 in light scatter mode and the detection threshold was set at 3 for maximum sensitivity with a minimum of background noise for all experiments.

2.9 | SYTOX™ Green staining

Cell death was detected via SYTOX™ Green nuclei staining. It can penetrate necrotic cells with a ruptured plasma membrane and bind to nuclei acids that result in green fluorescence. The experiment was performed as described previously (Geng, Wu, et al., 2020). H_2O_2

(400 μmol/L) was used as positive control. The images of SYTOX Green staining were quantified by their integrated fluorescent density. The area and intensity of the SYTOX Green staining were measured and the integrated density was calculated using ImageJ software. The quantification results are from three independent experiments.

2.10 | Statistical analysis

All results are presented as a mean of three to five independent experiments ±SD. For each assay, statistical analyses were performed using the Kruskal−Wallis test, followed by Dunn's multiple
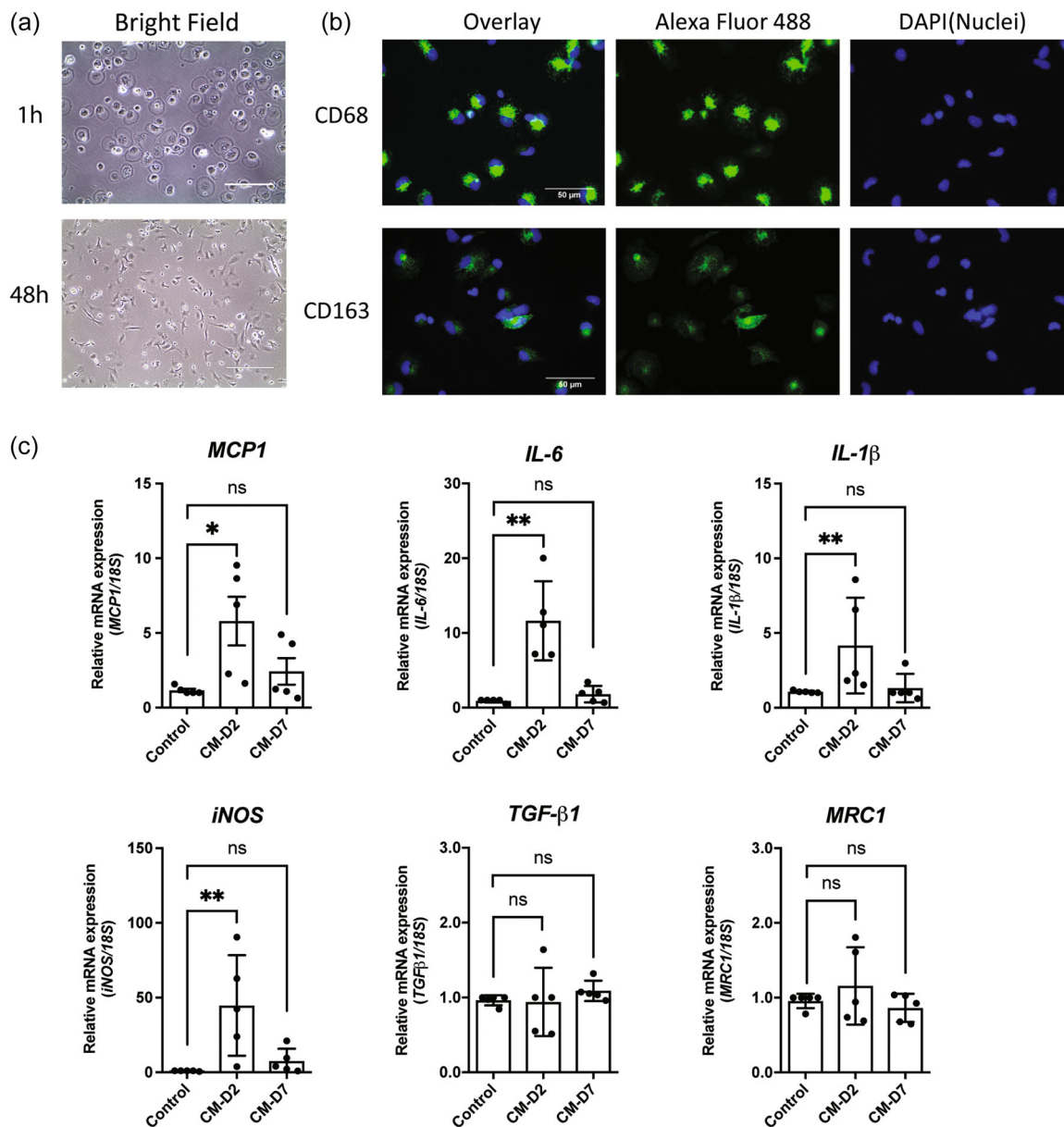

FIGURE 1 Conditioned medium (CM) of hepatic stellate cells (HSCs) induce inflammation in Kupffer cells (KCs). KCs were isolated from male Wistar rats and seeded in plastic plates. (a) Representative light microscopy picture was taken after 1 or 48 h of seeding. Scale bar: 100 μm. (b) KCs were incubated with anti-CD68 (ED1) or anti-CD163 (ED2) antibodies and subsequently stained with DAPI. Scale bar: 50 μm. (c) Conditioned media of HSCs were harvested from 4 h to 2 days (CM-D2) or from 5 to 7 days (CM-D7) after HSCs isolation. KCs were treated with CM-D2 or CM-D7 mixed with KC medium at a 1:1 (v/v) ratio for 24 h. Cells incubated with KC medium + HSC medium at a 1:1 (v/v) ratio served as control. mRNA expression of IL-6, IL-1β, iNOS, MCP1, TGF-β1, and MRC1 was measured by real-time quantitative PCR. Data are shown as mean ± SD. *$p < 0.05$, **$p < 0.01$, $^{ns}p > 0.05$.

comparison test or Newman−Keuls test; $p < 0.05$ was considered as statistically significant.

3 | RESULTS

3.1 | CM of HSCs induce an inflammatory phenotype in KCs

KCs were isolated from male Wistar rats. Shortly after attachment, they exhibited the Kupffer cell specific "fried eggs" shape. After 48 h incubation, KCs lost the "fried egg" shape but stayed adhesive to the plate with microvilli and pseudopodia present on the surface as shown in Figure 1a. To further check the purity of the cells, two specific Kupffer cell markers, CD68/ED1 and CD163/ED2, were examined. As shown in Figure 1b, the vast majority of the cells were positive for both CD68 and CD163.

HSCs were also isolated from male Wistar rats. Conditioned media of HSCs were harvested from Day 0 (excluding 4 h of attachment period) to 2 (CM-D2) or from Day 5 to 7 (CM-D7) after culture. KCs were treated with these conditioned media at 1:1 ratio mixed with KC medium for

24 h. After treatment, CM-D2 induced enhanced expression of proinflammatory mediators in KCs, demonstrated by significantly increased mRNA expression of the M1 markers: *MCP1, IL-6, IL-1β*, and *iNOS* ($p < 0.05$ or $p < 0.01$, Figure 1c), but no significant changes in the expression of the pro-fibrogenic gene *TGF-β1* or the M2 marker *MRC1* ($p > 0.05$). Interestingly, CM-D7 did not induce inflammation in KCs ($p > 0.05$, Figure 1c). In addition, rat hepatocyte-derived CM (CM-rHep) also did not induce KCs inflammation and even inhibited the inflammatory phenotype (Supporting Information: Figure 1).

3.2 | Conditioned media of HSCs do not modulate the phagocytosis of KCs

Since KCs are the most important phagocytes in the liver and play a critical role in the clearance of exogenous particles, we investigated whether the conditioned media affect their phagocytic ability. After treatment with CM for 24 h, KCs were incubated with FITC-labeled *E. coli* for 20 min, then fixed and stained with F-actin and DAPI. The number of *E. coli* engulfed per KC was counted. As shown in Figure 2a,b, CM-D2 and CM-D7 did not significantly influence the number of *E. coli* phagocytized
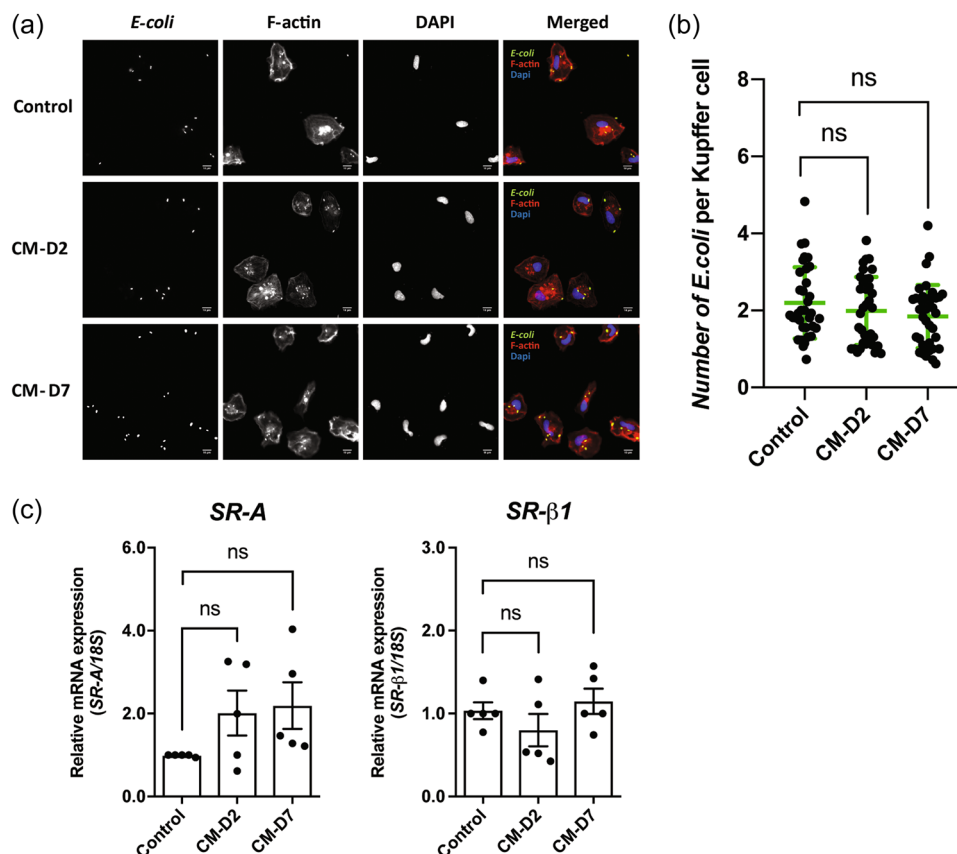

FIGURE 2 Conditioned media of HSCs do not influence phagocytosis of KCs. KCs were treated with CM-D2 or CM-D7 mixed with KC medium (1:1 [v/v]) for 24 h. (a) After treatment, KCs were incubated with FITC- labeled *E. coli* for 20 min, then fixed and stained with F-actin and DAPI. The phagocytic ability was measured by quantifying the engulfment of FITC-labeled *E. coli* in KCs using fluorescent microscopy. (b) The number of *E. coli* per KC was counted. Data were taken from three independent experiments and in total 36 images were measured. (c) mRNA expression of SR-a and SR-β1 was measured by real-time quantitative PCR. Data are shown as mean ± SD of three to five independent experiments. $^{ns}p > 0.05$. CM, conditioned medium; FITC, fluorescein isothiocyanate; HSCs, hepatic stellate cells; KCs, Kupffer cells.
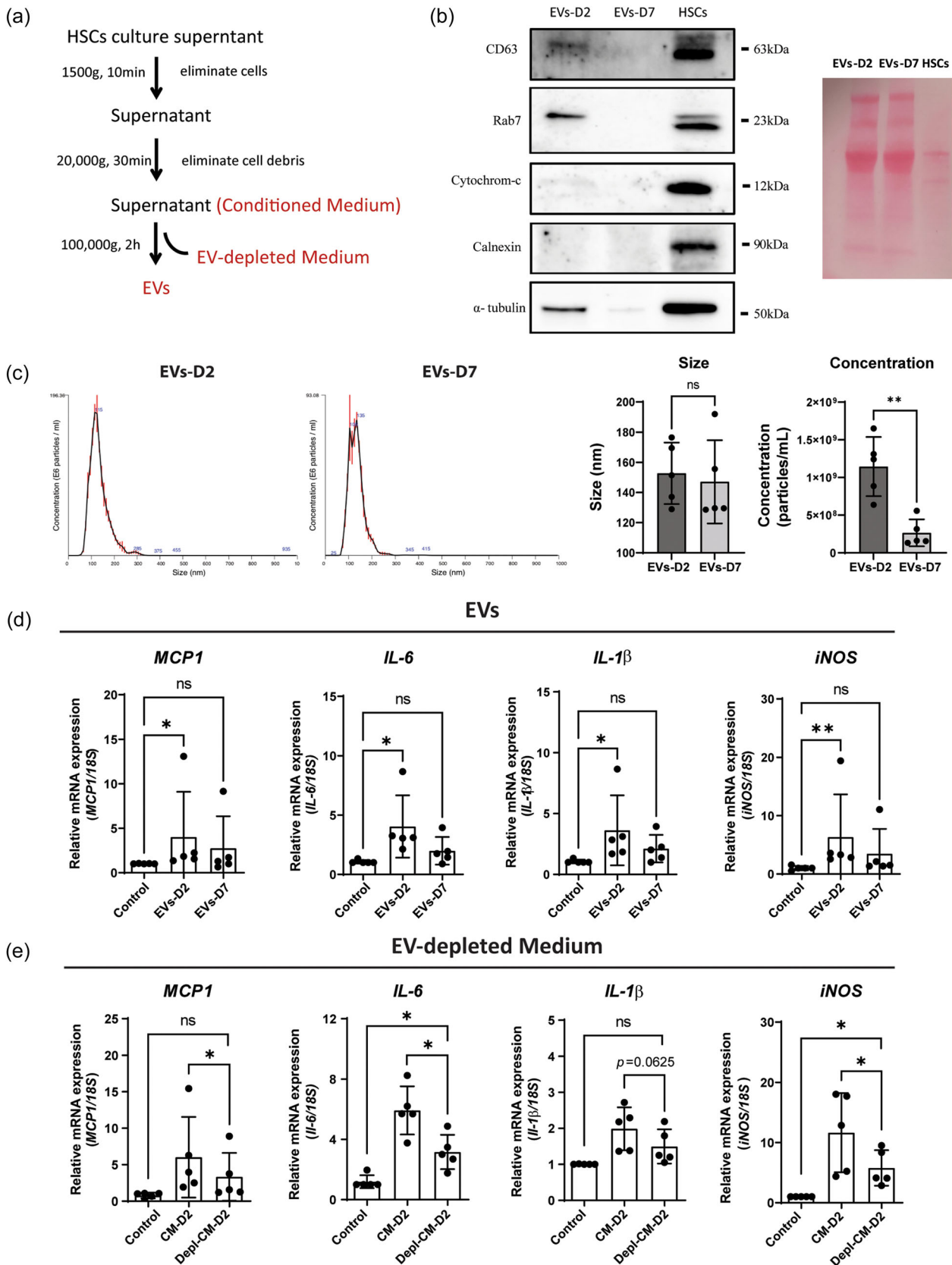
FIGURE 3 (See caption on next page).

by KCs ($p > 0.05$). Moreover, CM-D2 and CM-D7 also did not significantly affect the mRNA expression of scavenger receptors—*SR-a* and *SR-β1* ($p > 0.05$, Figure 2c). Therefore, the results indicate that conditioned media of HSCs do not influence the phagocytosis of bacteria by KCs.

3.3 | The proinflammatory effect of the CM is mediated by EVs released from HSCs

EVs were isolated from CM-D2 and CM-D7 via differential ultracentrifugation (Figure 3a). Western blot analysis results show that CM-D2 contains more EVs than CM-D7, indicated by the level of CD63, Rab7, and α-tubulin (Figure 3b). In addition, the purity of EVs was examined by the absence of cytochrome-*c* and calnexin as shown in Figure 3b. Moreover, NTA showed a significant lower concentration of particles from EVs-D7 compared to that of EVs-D2 ($p < 0.01$), whereas the average size of EVs-D2 and EVs-D7 were not significantly different (Figure 3c). Importantly, EVs-D2 (50 μg/mL), but not EVs-D7 (50 μg/mL), induced the proinflammatory M1-phenotype in KCs, demonstrated by the significantly increased mRNA expression of *MCP1*, *IL-6*, *IL-1β*, and *iNOS* ($p < 0.05$ or $p < 0.01$, Figure 3d), which correlates with the proinflammatory effects of conditioned media. Moreover, EVs depleted medium (Depl-CM-D2) exhibited a significantly reduced proinflammatory effect on KCs compared to the effect of CM-D2, as shown by the significantly decreased mRNA expression of *MCP1*, *IL-6*, and *iNOS* ($p < 0.05$, Figure 3e). These results imply that in the early stage of activation, HSCs release more EVs that induce KC inflammation than at later stages of activation. Of note, as shown in Figure 3e, Depl-CM-D2 did not significantly increase the expression of *MCP1* and *IL1β*, but significantly induced the expression of *IL-6* and *iNOS* ($p < 0.05$). Therefore, it is likely that there are mediators other than EVs that were still present in the EV-depleted medium and also induced M1 polarization of KCs.

3.4 | Inhibiting the activation of HSCs reduces the production of EVs

To investigate whether inhibiting the activation of HSCs would affect the production of EVs, quiescent HSCs, after attachment, were incubated in medium supplemented with chloroquine (CQ,

20 μmol/L) or DMSO. CQ was shown to suppress the activation of HSCs via inhibiting autophagy (He et al., 2014; Thoen et al., 2011). CQ (20 μmol/L) inhibited the activation of HSCs morphologically demonstrated by less stretching and less fibroblast-like shaped cells as shown in Figure 4a. Of note, CQ (20 μmol/L) did not induce cell death demonstrated by the lack of SYTOX Green nuclear staining as shown in Figure 4b. The inhibition of HSC activation by CQ was also demonstrated by significantly reduced intracellular protein levels of Collagen type 1 and αSMA and inhibition of autophagy demonstrated by increased LC3B-II and p62 levels compared to HSCs treated with DMSO (Figure 4c). Importantly, CQ treated HSCs showed reduced production of EVs demonstrated by the reduced particle concentration by NTA and reduced protein levels of CD63, Rab7, and α-Tubulin compared to HSCs treated with DMSO (Figure 4d,e). Meanwhile, the average size of EVs was not significantly changed (Figure 4d, $p > 0.05$).

3.5 | The proinflammatory effect of CM depends on TLR4 activation

As shown in Figure 5a, blocking the activation of TLR4 using a chemical TLR4 inhibitor (TAK242, 5 μmol/L) totally abolished the proinflammatory effects of CM-D2 on KCs, as shown by significantly reduced mRNA expressions of *MCP1*, *il-6*, *Il-1β*, and *iNOS* ($p < 0.01$ or $p < 0.001$). Furthermore, using a TLR4 reporter cell line, we found that CM-D2 but not CM-D7 significantly activated TLR4 ($p < 0.05$), which could be blocked by TAK-242 (Figure 5b). Similarly, the HSC-derived EVs, specifically EVs-D2, significantly activated TLR4 ($p < 0.05$), which could also be blocked by TAK-242 (Figure 5c). These results indicate that the proinflammatory effect of HSC-derived EVs is dependent on TLR4 activation in KCs.

4 | DISCUSSION AND CONCLUSIONS

Liver fibrosis is characterized by excessive deposition of ECM by HSCs. Under normal conditions, HSCs are quiescent and store lipids (vitamin A). In conditions of chronic liver injury, HSCs lose their lipid content, start to proliferate and produce large quantities of matrix proteins. It is believed that inflammatory cells, via cytokines, growth factors, and chemokines, modulate the process of HSC activation and hence, fibrogenesis (Friedman & Arthur, 1989; Shiratori et al., 1986; Zerbe & Gressner, 1988).

FIGURE 3 The proinflammatory effect of the CM on KCs is mediated by extracellular vesicles (EVs) released from HSCs. (a) Differential ultracentrifugation was used for EV purification. (b) Protein levels of CD63, Rab7, cytochrome-*c* (cyt-*c*), calnexin, and α-tubulin were measured in EVs purified from CM-D2 or CM-D7 (left). Equal protein loading was checked by Ponceau S staining. (right). (c) The size distribution and concentration of EVs were measured by nanoparticle tracking analysis (NTA). (d) KCs were treated with EVS-D2 (50 μg/mL) or EV-D7 (50 μg/mL) for 24 h. mRNA expressions of IL-6, IL-1β, iNOS, and MCP1 were measured by real-time quantitative PCR. (e) KCs were treated with CM-D2 or Depl-CM-D2 (mixed with KC medium [1:1 [v/v]]) for 24 h. mRNA expression of IL-6, IL-1β, iNOS, and MCP1 was measured by real-time quantitative PCR. Data are shown as mean ± SD. *$p < 0.05$, **$p < 0.01$, ns$p > 0.05$. CM, conditioned medium; HSCs, hepatic stellate cells; KCs, Kupffer cells.
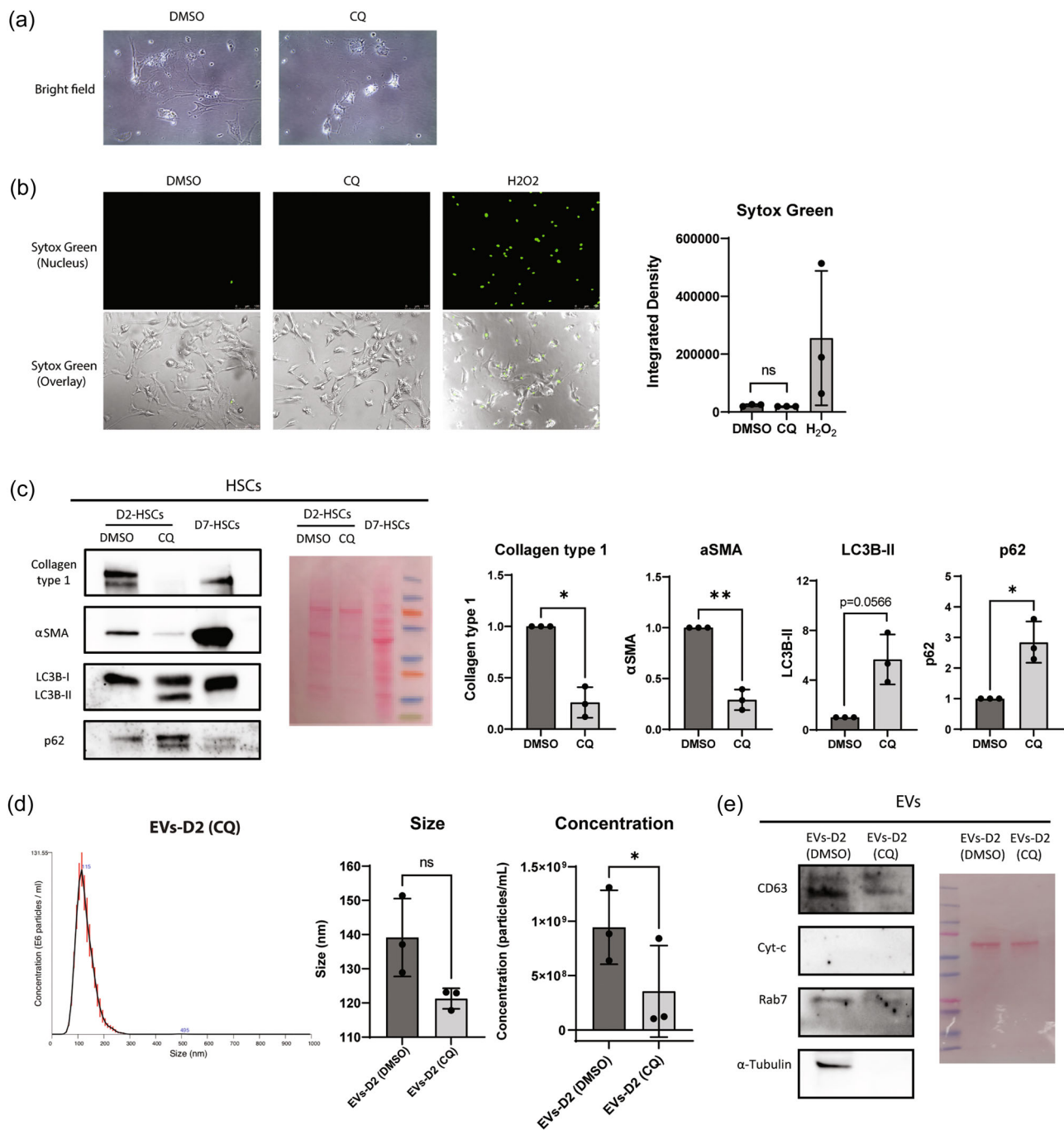
FIGURE 4 Inhibiting the activation of HSCs reduces the production of EVs. Freshly isolated HSCs were incubated in chloroquine (CQ, 20 µmol/L) or DMSO for 2 days. (a) Representative light microscopy pictures were taken. (b) Sytox green nuclei staining. H_2O_2 (400 µmol/L) was used as the positive control. The green fluorescent stain indicate dead cells. Scale bar: 100 µm. (c) Protein levels of collagen type 1, α-SMA, LC3B, and p62 were measured in HSCs (D2) treated with or without CQ, together with fully activated HSCs (D7) (left). Equal protein loading was checked by Ponceau S staining (right). The immunoblots were quantified by densitometry from three independent experiments. (d) The size distribution and concentration of EVs were measured by nanoparticle tracking analysis (NTA). (e) Protein levels of CD63, cytochrome-*c* (cyt-*c*), Rab7, and α-Tubulin were measured in EVs purified from HSCs (D2) treated with or without CQ (left). Equal protein loading was checked by Ponceau S staining. (right). EVs, extracellular vesicles; HSCs, hepatic stellate cells.

In the present study, we show that this intercellular communication is bidirectional and that HSCs, especially at an early stage of activation, induce a proinflammatory (M1) phenotype in KCs, mediated via the release of EVs, which is closely associated with the early activation of HSCs. Moreover, the proinflammatory effect of HSC-derived EVs is dependent on TLR4 activation. These results extend our understanding of the communication between HSCs and KCs and demonstrate the bidirectional communication between these two types of cells.
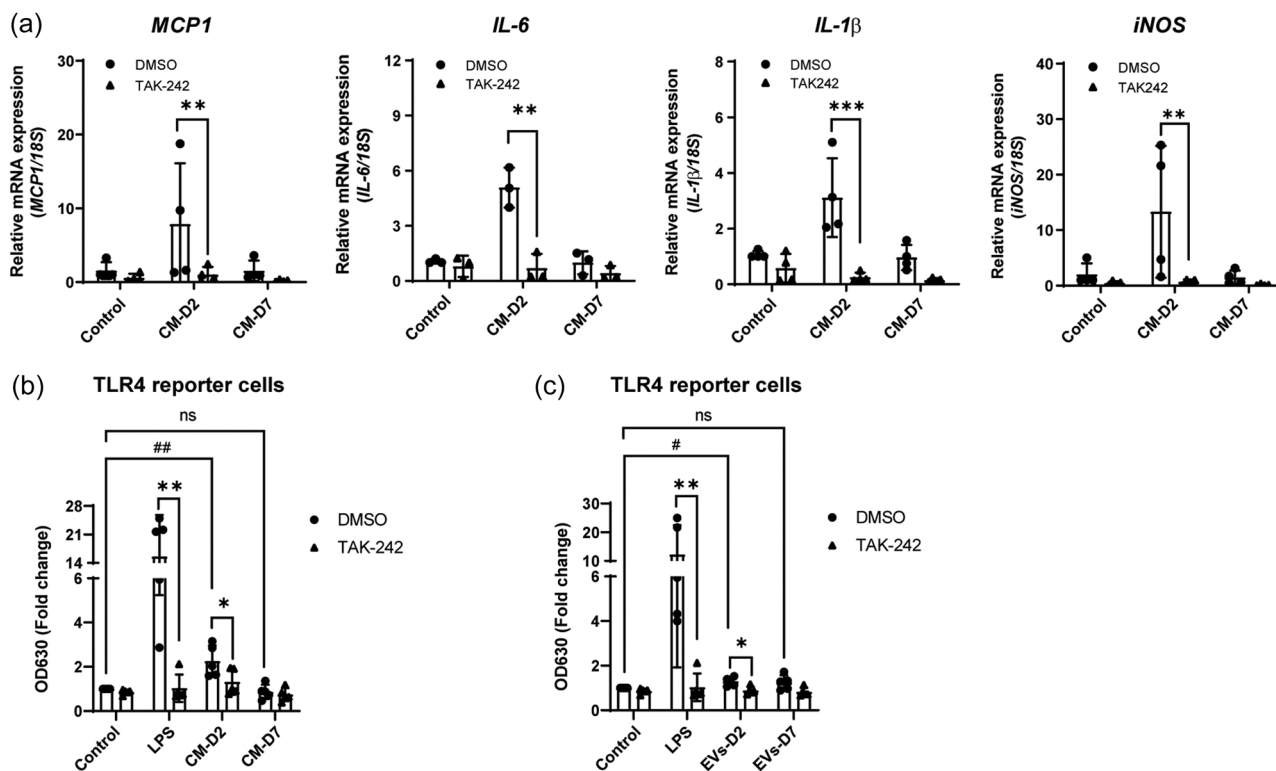
FIGURE 5 The proinflammatory effect of CM on KCs depends on TLR4 activation. (a) KCs were pretreated with TAK242 (5 µmol/L) for 10 min, and then incubated with CM-D2 or CM-D7 (mixed with KC medium [1:1 [v/v]]) in the presence or absence of TAK242 for 24 h. mRNA expressions of IL-6, IL-1β, iNOS, and MCP1 was measured by real-time quantitative PCR. (b) The activation of TLR4 by the CM was quantified using a TLR4 reporter cell line—HEK-Blue[TM] hTLR4 with the presence and absence of TLR4 inhibitor—TAK242 (5 µmol/L). (c) The activation of TLR4 by HSC-derived EVs (20 µg) was also quantified using a TLR4 reporter cell line—HEK-Blue[TM] hTLR4 with the presence and absence of TLR4 inhibitor—TAK242 (5 µmol/L). Data are shown as mean ± SD. *$p < 0.05$, **$p < 0.01$, ***$p < 0.001$, [ns]$p > 0.05$. CM, conditioned medium; EVs, extracellular vesicles; HSCs, hepatic stellate cells; KCs, Kupffer cells; TLR4, toll-like receptor 4.

As shown in this study, HSC-derived CM and EVs selectively induce the M1 inflammatory phenotype in KCs but do not significantly increase the expression of M2 markers MRC1 or TGF-β1 (Figure 1c). These results indicate that at the early stage of activation, HSC contribute to a proinflammatory microenvironment. However, macrophages are highly plastic cells. A study by Chang et al. observed that HSC-derived CM promoted a distinct macrophage differentiation profile, demonstrated by an IL-6^{high}/IL-10^{low}/TGF-β[high] phenotype, which cannot be simply categorized in the classic M1/M2 paradigm (Chang et al., 2013). The difference between our results and theirs might related to the use of cells of different origins: Chang et al. used the human HSC cell line (hTERT-HSC) and human peripheral blood mononuclear cell-derived macrophage, whereas we used primary rat HSC and primary rat KC. Furthermore, whether the phenotypic changes they observed are related to EVs were not described. In our study, we did not observe increased TGF-β1 expression in KCs, but mainly inflammatory genes belonging to M1 cytokines, which implies that the HSC-EV-exposed KCs might not directly promote HSCs activation via TGF-β1, but rather recruit monocyte infiltration thus promoting the progression of liver fibrosis. In hepatic fibrogenesis, the number of KCs decreases during the progression of liver injury whereas the number of infiltrating monocytes increases (Holt et al., 2008; Karlmark et al., 2009; Krenkel & Tacke, 2017; Sica

et al., 2014). These monocyte-derived macrophages constitute the major pro-fibrogenic macrophage population in the liver (Karlmark et al., 2009; Tacke & Zimmermann, 2014). Our results provide at least one mechanism (HSC-EVs) by which monocyte-derived macrophages are recruited into the liver in the early stages of fibrosis.

The effects of HSC-derived CM are related to the release of EVs. We showed that more EVs were present in CM-D2 compared to CM-D7, indicating that HSCs release more EVs at their early activation stage rather than the fully activated stage. It is important to speculate about the EV components (cargo) that are responsible for the observed effects. During activation, quiescent HSCs quickly lose their lipid content. These lipid droplets contain a large number of retinyl species (Lee et al., 2015; Molenaar et al., 2017; Testerink et al., 2012). Thus, we checked whether the inflammatory effects of HSC-derived CM were related to retinyl species. Direct exposure of KCs to retinoic acids (9-cis-retinoic acid [9cRA, 5 µmol/L], all-trans-retinoic acid [atRA, 5 µmol/L]) or retinol (5 µmol/L) did not induce the inflammatory phenotype in KCs (Supporting Information: Figure 2). Moreover, inhibition of retinoic acid synthesis by a chemical inhibitor of alcohol dehydrogenase (4-methylpyrazole [4MP, 2 mmol/L]) also did not modify the proinflammatory effect of HSC-derived CM (Supporting Information: Figure 2). Therefore, the effects of HSC-derived CM are

not related to retinoic acids or retinol. Furthermore, autophagy is an important cellular process that regulates the activation of HSCs (He et al., 2014; Thoen et al., 2011, 2012). Inhibiting the activation of quiescent HSCs by suppressing autophagy with CQ reduced the release of EVs from HSCs (Figure 4). This result further indicates that the relatively large amount of EVs production is a feature of the early activation of HSCs. Noticeably, a study from Gao et al. showed that inhibiting autophagy via activation of mTOR (mammalian target of rapamycin) signaling promoted EV release in HSCs (Gao et al., 2020). However, whether stimulating mTOR signaling affected the activation of HSCs and at which activation stage the cells were used were not mentioned. Therefore, it is important to investigate in detail the roles of autophagy on the release of HSC-derived EVs.

Additionally, we observed that the proinflammatory effects of HSC-derived CM and EVs are dependent on the activation of TLR4 (Figure 5). Moreover, inhibition of NF-κB or mTOR, by MG132 or rapamycin respectively, also abolished the proinflammatory effects of HSC-derived CM (data not shown). These results indicate that the cargo of HSC-derived EVs contains ligands of TLR4 that mediate the proinflammatory effects of HSC-CM/EVs on KCs. In this respect it is interesting to refer to a study from Kostallari et al. who showed that the pro-fibrogenic action of HSC-derived EVs is due to the presence of PDGFRα in EVs (Kostallari et al., 2018). Future studies will investigate the identity of molecules presenting in our HSC-derived EVs that are responsible for the observed proinflammatory effects.

In conclusion, in the present study, we showed that HSC-derived EVs induce a proinflammatory M1 phenotype in KCs, which is dependent on TLR4 activation. Moreover, this proinflammatory effect is only present in EVs derived from HSCs in the early stage of activation.

AUTHOR CONTRIBUTIONS

Yana Geng: Conceptualization, investigation, methodology, formal analysis, data curation, writing—original draft. **Junyu Wang**: Investigation, methodology, writing—review and editing. **Sandra Alejandra Serna-Salas**: Investigation. **Alejandra Hernández Villanueva**: Methodology. **Manon Buist-Homan**: Investigation, methodology. **Marco Arrese**: Methodology. **Peter Olinga**: Resources. **Hans Blokzijl**: Funding acquisition, supervision. **Han Moshage**: Conceptualization, funding acquisition, supervision, writing—review and editing, project administration.

ACKNOWLEDGMENTS

CONFLICT OF INTEREST STATEMENT

The authors declare no conflict of interest.

ORCID

Yana Geng http://orcid.org/0000-0003-1529-0875
Junyu Wang http://orcid.org/0000-0003-4605-2423

REFERENCES

Balaphas, A., Meyer, J., Sadoul, R., Morel, P., Gonelle-Gispert, C., & Bühler, L. H. (2019). Extracellular vesicles: Future diagnostic and therapeutic tools for liver disease and regeneration. *Liver International*, 39(10), 1801–1817.

Chang, J., Hisamatsu, T., Shimamura, K., Yoneno, K., Adachi, M., Naruse, H., Igarashi, T., Higuchi, H., Matsuoka, K., Kitazume, M. T., Ando, S., Kamada, N., Kanai, T., & Hibi, T. (2013). Activated hepatic stellate cells mediate the differentiation of macrophages. *Hepatology Research*, 43(6), 658–669.

Charrier, A., Chen, R., Chen, L., Kemper, S., Hattori, T., Takigawa, M., & Brigstock, D. R. (2014). Exosomes mediate intercellular transfer of pro-fibrogenic connective tissue growth factor (CCN2) between hepatic stellate cells, the principal fibrotic cells in the liver. *Surgery*, 156(3), 548–555.

Devaraj, E., Perumal, E., Subramaniyan, R., & Mustapha, N. (2022). Liver fibrosis: Extracellular vesicles mediated intercellular communication in perisinusoidal space. *Hepatology*, 76(1), 275–285.

Friedman, S. L., & Arthur, M. J. (1989). Activation of cultured rat hepatic lipocytes by Kupffer cell conditioned medium. Direct enhancement of matrix synthesis and stimulation of cell proliferation via induction of platelet-derived growth factor receptors. *Journal of Clinical Investigation*, 84(6), 1780–1785.

Gao, J., Wei, B., de Assuncao, T. M., Liu, Z., Hu, X., Ibrahim, S., Cooper, S. A., Cao, S., Shah, V. H., & Kostallari, E. (2020). Hepatic stellate cell autophagy inhibits extracellular vesicle release to attenuate liver fibrosis. *Journal of Hepatology*, 73(5), 1144–1154.

Geng, Y., Arroyave-Ospina, J. C., Buist-Homan, M., Plantinga, J., Olinga, P., Reijngoud, D. J., Van Vilsteren, F. G. I., Blokzijl, H., Kamps, J. A. A. M., & Moshage, H. (2023). Differential effects of oleate on vascular endothelial and liver sinusoidal endothelial cells reveal its toxic features in vitro. *The Journal of Nutritional Biochemistry*, 114, 109255.

Geng, Y., Hernández Villanueva, A., Oun, A., Buist-Homan, M., Blokzijl, H., Faber, K. N., Dolga, A., & Moshage, H. (2020). Protective effect of metformin against palmitate-induced hepatic cell death. *Biochimica et Biophysica Acta (BBA)-Molecular Basis of Disease*, 1866(3), 165621.

Geng, Y., Wu, Z., Buist-Homan, M., Blokzijl, H., & Moshage, H. (2020). Hesperetin protects against palmitate-induced cellular toxicity via induction of GRP78 in hepatocytes. *Toxicology and Applied Pharmacology*, 404, 115183.

Hernández, A., Geng, Y., Sepúlveda, R., Solís, N., Torres, J., Arab, J. P., Barrera, F., Cabrera, D., Moshage, H., & Arrese, M. (2020). Chemical hypoxia induces pro-inflammatory signals in fat-laden hepatocytes and contributes to cellular crosstalk with Kupffer cells through extracellular vesicles. *Biochimica et Biophysica Acta (BBA)-Molecular Basis of Disease*, 1866(6), 165753.

Hernández, A., Reyes, D., Geng, Y., Arab, J. P., Cabrera, D., Sepulveda, R., Solis, N., Buist-Homan, M., Arrese, M., & Moshage, H. (2020). Extracellular vesicles derived from fat-laden hepatocytes undergoing chemical hypoxia promote a pro-fibrotic phenotype in hepatic stellate cells. *Biochimica et Biophysica Acta (BBA)-Molecular Basis of Disease*, 1866(10), 165857.

He, W., Wang, B., Yang, J., Zhuang, Y., Wang, L., Huang, X., & Chen, J. (2014). Chloroquine improved carbon tetrachloride-induced liver fibrosis through its inhibition of the activation of hepatic stellate cells: Role of autophagy. *Biological and Pharmaceutical Bulletin*, 37(9), 1505–1509.

Holt, M. P., Cheng, L., & Ju, C. (2008). Identification and characterization of infiltrating macrophages in acetaminophen-induced liver injury. *Journal of Leukocyte Biology*, 84(6), 1410–1421.

Inzaugarat, M. E., Wree, A., & Feldstein, A. E. (2016). Hepatocyte mitochondrial DNA released in microparticles and toll-like receptor 9 activation: A link between lipotoxicity and inflammation during nonalcoholic steatohepatitis. *Hepatology*, 64(2), 669–671.

Jiang, J. X., Mikami, K., Shah, V. H., & Torok, N. J. (2008). Leptin induces phagocytosis of apoptotic bodies by hepatic stellate cells via a Rho guanosine triphosphatase-dependent mechanism. *Hepatology*, *48*(5), 1497–1505.

Karlmark, K. R., Weiskirchen, R., Zimmermann, H. W., Gassler, N., Ginhoux, F., Weber, C., Merad, M., Luedde, T., Trautwein, C., & Tacke, F. (2009). Hepatic recruitment of the inflammatory Gr1+ monocyte subset upon liver injury promotes hepatic fibrosis. *Hepatology*, *50*(1), 261–274.

Kostallari, E., Hirsova, P., Prasnicka, A., Verma, V. K., Yaqoob, U., Wongjarupong, N., Roberts, L. R., & Shah, V. H. (2018). Hepatic stellate cell-derived platelet-derived growth factor receptor-alpha-enriched extracellular vesicles promote liver fibrosis in mice through SHP2. *Hepatology*, *68*(1), 333–348.

Krenkel, O., & Tacke, F. (2017). Liver macrophages in tissue homeostasis and disease. *Nature Reviews Immunology*, *17*(5), 306–321.

Lee, Y. A., Wallace, M. C., & Friedman, S. L. (2015). Pathobiology of liver fibrosis: A translational success story. *Gut*, *64*(5), 830–841.

Molenaar, M. R., Vaandrager, A. B., & Helms, J. B. (2017). Some lipid droplets are more equal than others: Different metabolic lipid droplet pools in hepatic stellate cells. *Lipid Insights*, *10*, 117863531774728.

Moshage, H., Casini, A., & Lieber, C. S. (1990). Acetaldehyde selectively stimulates collagen production in cultured rat liver fat-storing cells but not in hepatocytes. *Hepatology*, *12*(3 Pt 1), 511–518.

Pellicoro, A., Ramachandran, P., Iredale, J. P., & Fallowfield, J. A. (2014). Liver fibrosis and repair: Immune regulation of wound healing in a solid organ. *Nature Reviews Immunology*, *14*(3), 181–194.

Povero, D., Panera, N., Eguchi, A., Johnson, C. D., Papouchado, B. G., de Araujo Horcel, L., Pinatel, E. M., Alisi, A., Nobili, V., & Feldstein, A. E. (2015). Lipid-induced hepatocyte-derived extracellular vesicles regulate hepatic stellate cells via MicroRNA targeting peroxisome proliferator-activated receptor-γ. *Cellular and Molecular Gastroenterology and Hepatology*, *1*(6), 646–663.

Shiratori, Y., Geerts, A., Ichida, T., Kawase, T., & Wisse, E. (1986). Kupffer cells from CCl4-induced fibrotic livers stimulate proliferation of fat-storing cells. *Journal of Hepatology*, *3*(3), 294–303.

Sica, A., Invernizzi, P., & Mantovani, A. (2014). Macrophage plasticity and polarization in liver homeostasis and pathology. *Hepatology*, *59*(5), 2034–2042.

Tacke, F., & Zimmermann, H. W. (2014). Macrophage heterogeneity in liver injury and fibrosis. *Journal of Hepatology*, *60*(5), 1090–1096.

Testerink, N., Ajat, M., Houweling, M., Brouwers, J. F., Pully, V. V., van Manen, H. J., Otto, C., Helms, J. B., & Vaandrager, A. B. (2012). Replacement of retinyl esters by polyunsaturated triacylglycerol species in lipid droplets of hepatic stellate cells during activation. *PLoS One*, *7*(4), e34945.

Thoen, L. F. R., Guimarães, E. L. M., Dollé, L., Mannaerts, I., Najimi, M., Sokal, E., & van Grunsven, L. A. (2011). A role for autophagy during hepatic stellate cell activation. *Journal of Hepatology*, *55*(6), 1353–1360.

Thoen, L. F. R., Guimarães, E. L., & van Grunsven, L. A. (2012). Autophagy: A new player in hepatic stellate cell activation. *Autophagy*, *8*(1), 126–128.

Viñas, O., Bataller, R., Sancho-Bru, P., Ginès, P., Berenguer, C., Enrich, C., Nicolás, J. M., Ercilla, G., Gallart, T., Vives, J., Arroyo, V., & Rodés, J. (2003). Human hepatic stellate cells show features of antigen-presenting cells and stimulate lymphocyte proliferation. *Hepatology*, *38*(4), 919–929.

Vrenken, T. E., Buist-Homan, M., Kalsbeek, A. J., Faber, K. N., & Moshage, H. (2008). The active metabolite of leflunomide, A77 1726, protects rat hepatocytes against bile acid-induced apoptosis. *Journal of Hepatology*, *49*(5), 799–809.

Wang, R., Ding, Q., Yaqoob, U., de Assuncao, T. M., Verma, V. K., Hirsova, P., Cao, S., Mukhopadhyay, D., Huebert, R. C., & Shah, V. H. (2015). Exosome adherence and internalization by hepatic stellate cells triggers sphingosine 1-phosphate-dependent migration. *Journal of Biological Chemistry*, *290*(52), 30684–30696.

Wang, S., Li, K., Pickholz, E., Dobie, R., Matchett, K. P., Henderson, N. C., Carrico, C., Driver, I., Borch Jensen, M., Chen, L., Petitjean, M., Bhattacharya, D., Fiel, M. I., Liu, X., Kisseleva, T., Alon, U., Adler, M., Medzhitov, R., & Friedman, S. L. (2023). An autocrine signaling circuit in hepatic stellate cells underlies advanced fibrosis in nonalcoholic steatohepatitis. *Science Translational Medicine*, *15*(677), eadd3949.

Xu, R., Zhang, Z., & Wang, F. S. (2012). Liver fibrosis: Mechanisms of immune-mediated liver injury. *Cellular & molecular immunology*, *9*(4), 296–301.

Zerbe, O., & Gressner, A. M. (1988). Proliferation of fat-storing cells is stimulated by secretions of Kupffer cells from normal and injured liver. *Experimental and Molecular Pathology*, *49*(1), 87–101.

Zhan, S. S., Jiang, J. X., Wu, J., Halsted, C., Friedman, S. L., Zern, M. A., & Torok, N. J. (2006). Phagocytosis of apoptotic bodies by hepatic stellate cells induces NADPH oxidase and is associated with liver fibrosis in vivo. *Hepatology*, *43*(3), 435–443.

SUPPORTING INFORMATION

Additional supporting information can be found online in the Supporting Information section at the end of this article.